

## Supporting Information

### **Guest-induced gate-opening in a flexible MOF adsorbent that exhibits benzene/cyclohexane selectivity**

Guo-Ao Li,<sup>a,†</sup> Min Deng,<sup>a,†</sup> Wei Guo,<sup>a</sup> Shuang Yin,<sup>a</sup> Yan-E Liu,<sup>a</sup> Ai-Xin Zhu<sup>\*a</sup> and Michael J. Zaworotko<sup>\*b</sup>

<sup>a</sup> Faculty of Chemistry and Chemical Engineering, Yunnan Normal University, Kunming 650500, China. Email: zaxchem@126.com

<sup>b</sup> Department of Chemical Sciences, Bernal Institute, University of Limerick, Limerick V94T9PX, Ireland. Email: xtal@ul.ie

# Contents

1. Materials and synthesis
2. Single-crystal X-ray diffraction measurements
3. Single-crystal data and structural parameters
4. Summary tables of weak interactions in the  $\alpha$  and  $\beta$  phases of X-pcu-11-Zn and Bz@X-pcu-11-Zn.
5. Supporting structure figures
6. Thermogravimetric analysis (TGA)
7. IR spectra
8. Powder X-ray diffraction (PXRD)
9. Gas and vapour adsorption measurements
10. The calculation of Langmuir surface area
11. Time-dependent, single-component Bz/Cy adsorption experiments
12. Time-dependent, binary-component Bz/Cy adsorption experiments
13. Cycling tests of Bz adsorption
14. Binary-component Bz/Cy adsorption experiments by gas chromatography
15. Kinetic analysis for Bz adsorption
16. Summary of switching and breathing metal-organic materials

## 1. Materials and synthesis

The ligands H<sub>2</sub>DMTDC was synthesized according to the literature methods.<sup>1</sup> Other reagents and solvents were commercially available and used without further purification.

**Synthesis of [Zn<sub>2</sub>(DMTDC)<sub>2</sub>(dpb)] 5DMF 0.5H<sub>2</sub>O (X-pcu-11-Zn- $\alpha$ ).** A mixture of Zn(NO<sub>3</sub>)<sub>2</sub>·6H<sub>2</sub>O (30 mg, 0.1 mmol), H<sub>2</sub>DMTDC (26 mg, 0.1 mmol), dpb (11 mg, 0.05 mmol), DMF (4 mL) was added to a 30 mL glass vial and then was ultrasonicated for 30 seconds. The vial was capped tightly and placed in an oven at 105 °C. After 24 hours, the vials were removed from the oven and allowed to cool to room temperature. Pale yellow, rod-shaped crystals were harvested by filtration and washed with DMF (Yield: 54%). IR (cm<sup>-1</sup>): 3437(br, m), 2925(m), 1668(s), 1616(s), 1499(s), 1438(w), 1370(s), 1225(m), 1150(w), 1096(m), 1024(m), 865(w), 810(s), 785(s), 723(m), 661(m), 613(m), 573(w), 488(w).

**Synthesis of [Zn<sub>2</sub>(DMTDC)<sub>2</sub>(dpb)] (X-pcu-11-Zn- $\beta$ ).** As-synthesized X-pcu-11-Zn- $\alpha$  was heated at 120 °C under vacuum for 12 h to afford X-pcu-11-Zn- $\beta$ . IR (cm<sup>-1</sup>): 3434(br, m), 2918(m), 1616(s), 1568(s), 1493(s), 1377(w), 1222(s), 1149(m), 1071(w), 1023(m), 864(w), 811(s), 779(s), 721(m), 611(m), 572(w), 484(w).

**Synthesis of [Zn<sub>2</sub>(DMTDC)<sub>2</sub>(dpb)]·3.5benzene (Bz@X-pcu-11-Zn).** The single-crystals of Bz@X-pcu-11-Zn was obtained by immersing as-synthesized X-pcu-11-Zn- $\alpha$  in benzene for two weeks afford Bz@X-pcu-11-Zn. IR (cm<sup>-1</sup>): 3423(br, m), 2920(m), 1614(s), 1572(s), 1499(m), 1379(s), 1223(m), 1154(w), 1071(m), 1026(m), 864(w), 813(s), 781(s), 724(m), 613(m), 574(w), 488(m).

## 2. Single-crystal X-ray diffraction measurements

Single crystals of X-pcu-11-Zn- $\alpha$  are prone to lose guest molecules in air at room temperature. Therefore, the crystals of X-pcu-11-Zn- $\alpha$  were dipped immediately in paraffin

oil after removal from mother liquor and subsequently mounted on mounting loop and kept under liquid N<sub>2</sub> flow. The crystal of **Bz@X-pcu-11-Zn** is prone to lose benzene to become opaque in air, so a block-like single crystal of **Bz@X-pcu-11-Zn** was promptly sealed in a capillary tube under an optical microscope with benzene inside. Diffraction intensities of the compounds **X-pcu-11-Zn- $\alpha$** , **X-pcu-11-Zn- $\beta$**  were collected on a Bruker Quest CCD diffractometer with graphite-monochromated Cu K $\alpha$  ( $\lambda = 1.54178\text{\AA}$ ) radiation. The data of **X-pcu-11-Zn- $\alpha$**  and **X-pcu-11-Zn- $\beta$**  was indexed, integrated and scaled in APEX3.<sup>2</sup> Absorption correction was performed by multi-scan method using in SADABS.<sup>3</sup> Diffraction intensities of **Bz@X-pcu-11-Zn** were collected at room temperature on a Rigaku R-Axis SPIDER diffractometer with graphite-monochromated Mo K $\alpha$  radiation ( $\lambda = 0.71073\text{ \AA}$ ). Absorption corrections were applied through the multi-scan program ABSCOR.<sup>4</sup> All the structures were solved using intrinsic phasing method (SHELXT)<sup>5</sup> and refined on  $F^2$  using nonlinear least-squares techniques with SHELXL programs.<sup>6</sup> Anisotropic thermal parameters were applied to all non-hydrogen atoms. All the hydrogen atoms were generated geometrically. In **X-pcu-11-Zn- $\beta$** , half of DMTDC ligands and one of pyridine ring from dpb ligands are disorder within two positions. In **Bz@X-pcu-11-Zn**, the benzene moieties from dpb ligands are disordered in two positions. The occupancies for all the disordered atoms in **X-pcu-11-Zn- $\beta$**  and **Bz@X-pcu-11-Zn** were refine in SHELX using PART commands with free variables. Other commands SADI, ISOR, and FLAT were used to restrain the geometry of disorder. The large volume fractions of disordered solvents in the lattice pores of **X-pcu-11-Zn- $\alpha$**  could not be modelled in terms of atomic sites and were treated using the SQUEEZE routine in the PLATON software package.<sup>7</sup> The void volume (excluding guest molecules) in the crystal cell was calculated using the program PLATON.<sup>7</sup> Crystallographic data and structural refinement information are listed in Tables S1. Crystallographic data for the structures reported in this

paper have been deposited with the Cambridge Crystallographic Data Centre as **CCDC** numbers 2372920-2372922 for **X-pcu-11-Zn- $\alpha$** , **X-pcu-11-Zn- $\beta$** , and **Bz@X-pcu-11-Zn**, respectively.



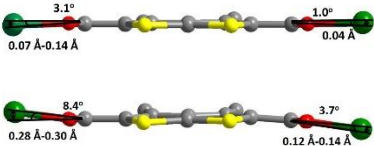

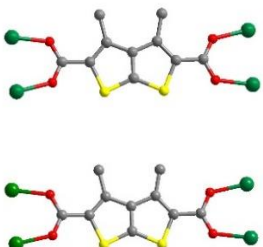

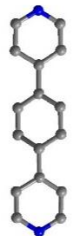
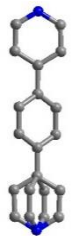
### 3. Single-crystal data and structural parameters

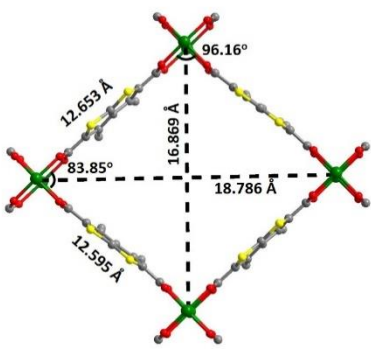
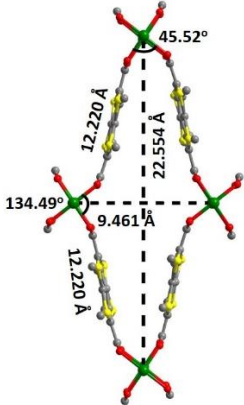
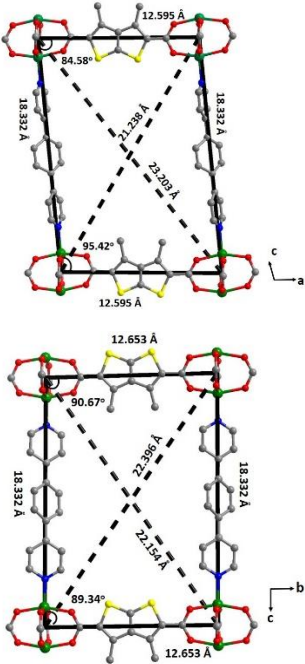
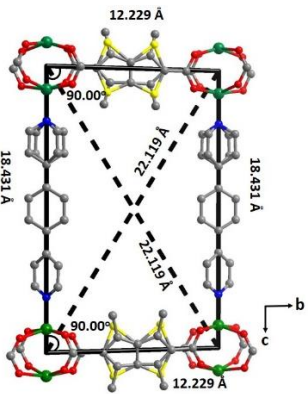
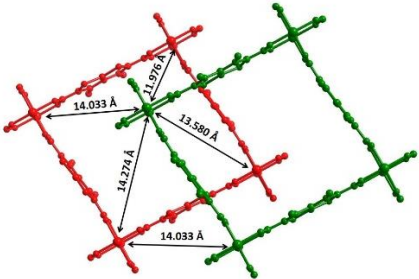
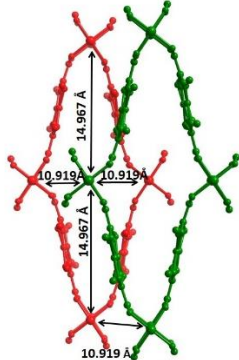
**Table S1.** Crystallographic data and structure refinement summary for **X-pcu-11-Zn**.

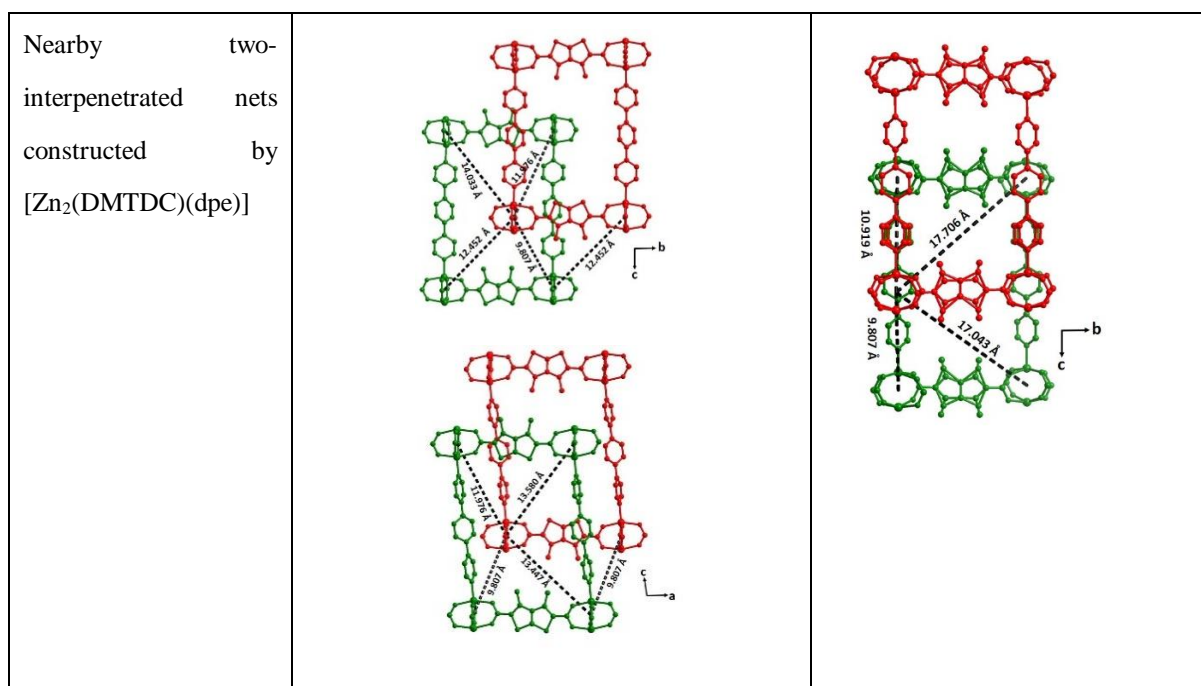
Compounds	<b>X-pcu-11-Zn-<math>\alpha</math></b>	<b>X-pcu-11-Zn-<math>\beta</math></b>	<b>Bz@X-pcu-11-Zn</b>
Formula	C <sub>36</sub> H <sub>24</sub> N <sub>2</sub> O <sub>8</sub> S <sub>4</sub> Zn <sub>2</sub> [+Solvent]	C <sub>36</sub> H <sub>24</sub> N <sub>2</sub> O <sub>8</sub> S <sub>4</sub> Zn <sub>2</sub>	C <sub>57</sub> H <sub>45</sub> N <sub>2</sub> O <sub>8</sub> S <sub>4</sub> Zn <sub>2</sub>
Formula weight	1246.11	871.55	1144.93
Crystal system	Triclinic	Orthorhombic	Triclinic
Space group	<i>P</i> -1	<i>Ibca</i>	<i>P</i> -1
<i>a</i> (Å)	12.5951(10)	9.4610(7)	12.623(3)
<i>b</i> (Å)	12.6532(10)	22.5537(14)	12.679(3)
<i>c</i> (Å)	18.3323(15)	36.862(2)	18.392(4)
$\alpha$ (deg)	90.665(4)	90	90.40(3)
$\beta$ (deg)	95.424(4)	90	98.91(3)
$\gamma$ (deg)	96.155(4)	90	95.74(3)
<i>V</i> (Å <sup>3</sup> )	2891.0(4)	7865.5(9)	2892.8(10)
<i>Z</i>	2	8	2
<i>D</i> <sub>c</sub> (g·cm <sup>-3</sup> )	1.431	1.472	1.314
$\mu$ (mm <sup>-1</sup> )	2.933	3.915	1.025
<i>R</i> <sub>int</sub>	0.0737	0.0618	0.0373
GOF	1.030	1.042	1.061
<i>R</i> <sub>1</sub> [ <i>I</i> > 2σ ( <i>I</i> )]	0.0781	0.0359	0.0565
<i>WR</i> <sub>2</sub> [ <i>I</i> > 2σ ( <i>I</i> )]	0.2240	0.1019	0.1561
<i>R</i> <sub>1</sub> [all data]	0.0866	0.0391	0.0812
<i>WR</i> <sub>2</sub> [all data]	0.2324	0.1051	0.1767
Diff peak, hole (e Å <sup>-3</sup> )	1.328, -0.939	0.353, -0.451	1.082, -0.920
No. CCDC	2372920	2372921	2372922

$$R_1 = \sum ||F_o| - |F_c|| / \sum |F_o|, \quad wR_2 = [\sum w(F_o^2 - F_c^2)^2 / \sum w(F_o^2)^2]^{1/2}$$

**Table S2.** Comparative analysis of structural differences between **X-pcu-11-Zn- $\alpha$**  and **X-pcu-11-Zn- $\beta$** .

Compounds	X-pcu-11-Zn- $\alpha$	X-pcu-11-Zn- $\beta$
Coordination geometry of Zn <sub>2</sub> units	 <p>Zn-O: 2.023(3)-2.050(4) Å  Zn-N: 2.037(4) / 2.040(4) Å  <math>\angle</math>O-Zn-O: 87.36(17)<math>^\circ</math>-160.04(16)<math>^\circ</math>  <math>\angle</math>N-Zn-O: 97.67(16)<math>^\circ</math>-102.66(16)<math>^\circ</math></p>	 <p>Zn-O: 2.0347(15)-2.0675(15) Å  Zn-N: 2.028(3) / 2.046(3) Å  <math>\angle</math>O-Zn-O: 84.12(7)<math>^\circ</math>-165.69(9)<math>^\circ</math>  <math>\angle</math>N-Zn-O: 97.15(4)<math>^\circ</math>-104.99(5)<math>^\circ</math></p>
Geometry parameters between zinc ions and carboxylate plane	 <p>3.1<math>^\circ</math>, 0.07 Å-0.14 Å  1.0<math>^\circ</math>, 0.04 Å  8.4<math>^\circ</math>, 0.28 Å-0.30 Å  3.7<math>^\circ</math>, 0.12 Å-0.14 Å</p>	 <p>30.1<math>^\circ</math>, 0.97-1.04 Å  18.1<math>^\circ</math>, 0.60-0.63 Å</p>
DMTDC linker		
dpb linker (dihedral angles of pyridine and benzene ring)	 <p>No disorder  145.1<math>^\circ</math>/149.7<math>^\circ</math></p>	 <p>Disordered  32.1<math>^\circ</math>/32.8<math>^\circ</math>/35.2<math>^\circ</math></p>

<p>2D sql net constructed by <math>[\text{Zn}_2(\text{DMTDC})_2]</math></p>		
<p>2D net constructed by <math>[\text{Zn}_2(\text{DMTDC})(\text{dpb})]</math></p>		
<p>Nearby two-interpenetrated 2D nets constructed by <math>[\text{Zn}_2(\text{DMTDC})_2]</math></p>		



Note: The numbers in the diagrams showing the angles and distances between binuclear zinc units.

#### 4. Summary tables of weak interactions in the $\alpha$ and $\beta$ phases of X-pcu-11-Zn and Bz@X-pcu-11-Zn.

**Table S3.** Possible hydrogen bonds between the two-fold interpenetrated nets in X-pcu-11-Zn- $\alpha$ , X-pcu-11-Zn- $\beta$  and Bz@X-pcu-11-Zn phases.

	D-H	H $\cdots$ A	D $\cdots$ A	$\angle$ D-H $\cdots$ A
<b>X-pcu-11-Zn-<math>\alpha</math></b>				
C(9)-H(9A) $\cdots$ O(1)	0.96	2.26	2.983(7)	132
C(10)-H(10A) $\cdots$ O(3)	0.96	2.28	3.002(6)	131
C(19)-H(19A) $\cdots$ O(5)	0.96	2.19	2.931(8)	133
C(20)-H(20A) $\cdots$ O(7)	0.96	2.26	2.998(8)	133
<b>X-pcu-11-Zn-<math>\beta</math></b>				
C(9)-H(9A) $\cdots$ O(2)	0.96	2.29	3.004(4)	131
C(10)-H(10A) $\cdots$ O(4)	0.96	2.21	2.952(4)	133
C(18)-H(18A) $\cdots$ O(2)	0.93	2.53	3.129(3)	123
<b>Bz@X-pcu-11-Zn</b>				
C(10)-H(10A) $\cdots$ O(4)	0.96	2.24	2.987(6)	134
C(20)-H(20A) $\cdots$ O(7)	0.96	2.30	3.019(5)	132

Symmetry code: (a)  $-x+1, -y, -z+1$ ; (b)  $-x, -y+2, -z+1$ ; (c)  $-x+2, -y+1, -z$ .

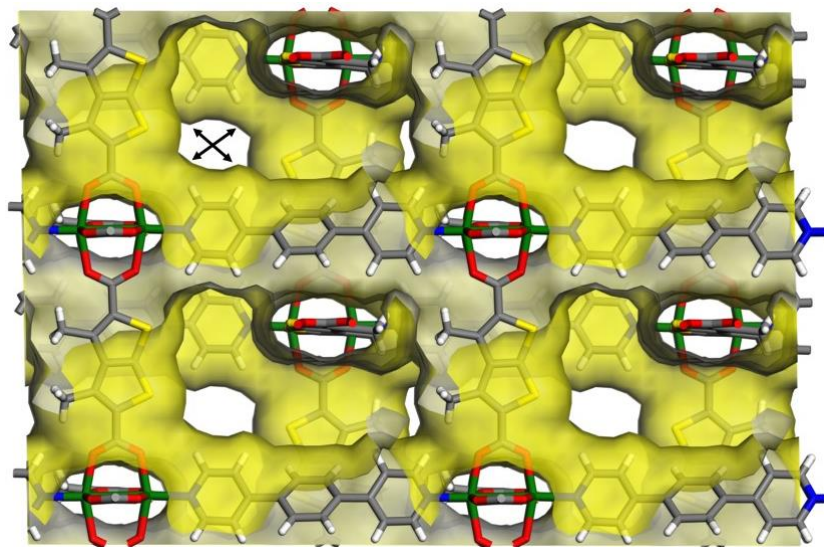
**Table S4.** Analysis of shortest aromatic stacking interaction in **Bz@X-pcu-11-Zn** phases.

	distance between ring centroids	distance between ring centroid to plane	distance between ring centroid to plane
thiophene-pyridine	3.851(3)	3.600(2)	3.325(2)
thiophene-benzene	3.681(5)	3.352(2)	3.522(4)

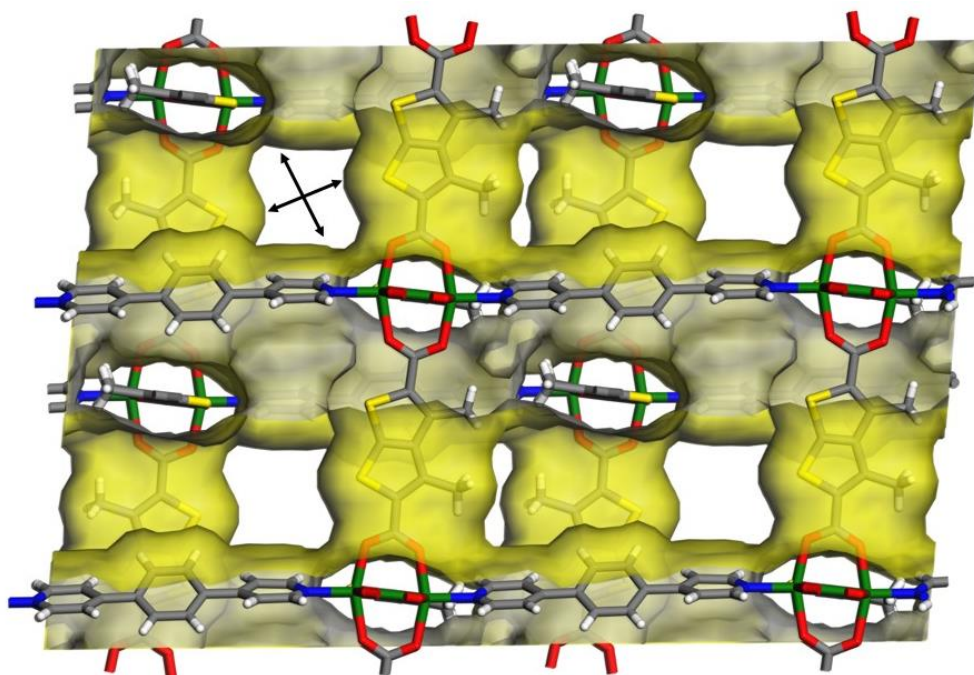
**Table S5.** Possible C-H  $\cdots \pi$  interactions in **Bz@X-pcu-11-Zn** phases.

	H $\cdots$ Cg	X $\cdots$ Cg	$\angle$ X-H $\cdots$ Cg
C(22)-H(22) $\cdots$ Cg	2.84	3.686(7)	152
C(52)-H(52) $\cdots$ Cg	2.90	3.679(15)	143
C(53)-H(53) $\cdots$ Cg	2.91	3.492(15)	122
C(54)-H(54) $\cdots$ Cg	2.82	3.626(12)	145
C(57)-H(57) $\cdots$ Cg	2.99	3.778(15)	144

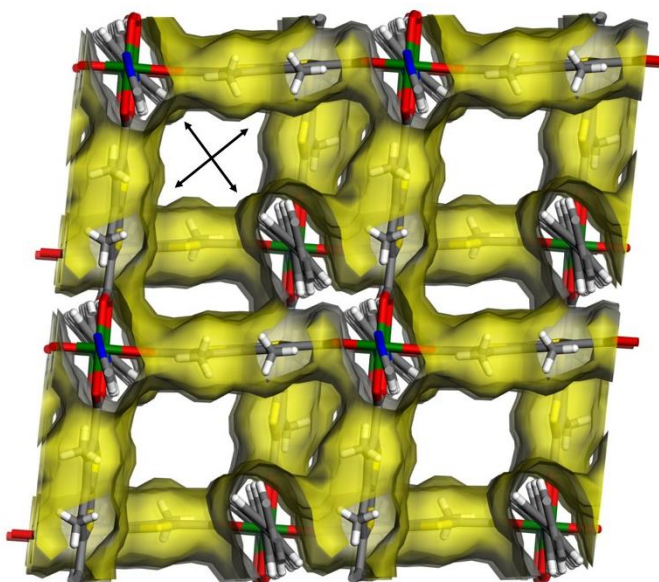
## 5. Supporting structure figures



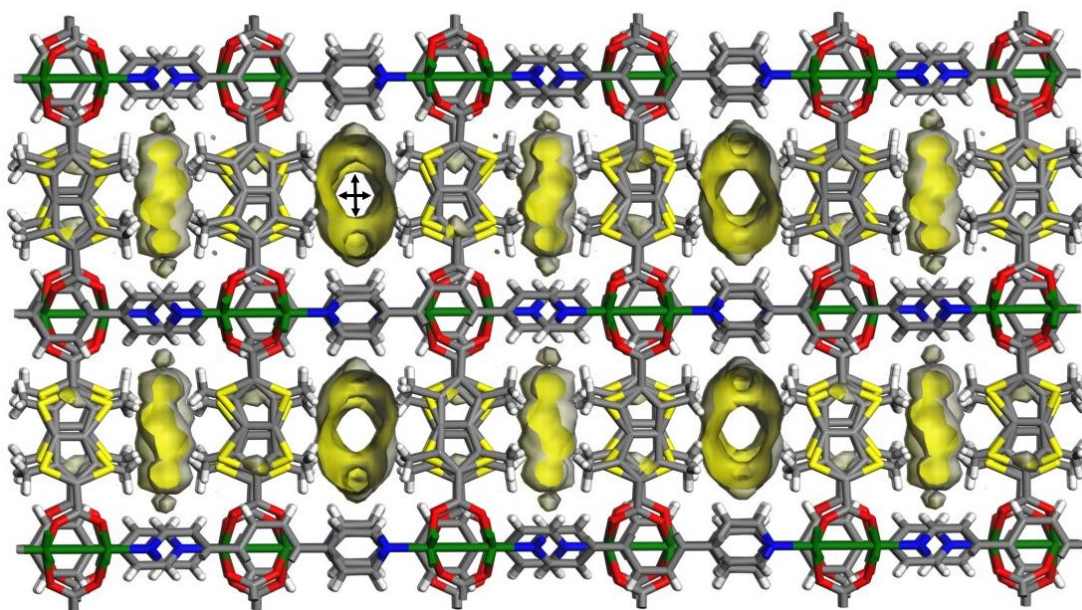
**Fig. S1** Illustrations of the position of pore diameters (approximately  $2.3 \times 2.5 \text{ \AA}^2$ , the direction is indicated by the arrows) viewed along the  $a$ -axis for **X-pcu-11-Zn- $\alpha$** .



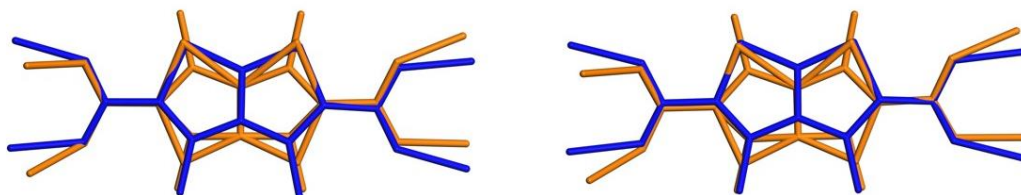
**Fig. S2** Illustrations of the position of pore diameters (approximately  $3.3 \times 5.4 \text{ \AA}^2$ , the direction is indicated by the arrows) viewed along the *b*-axis for **X-pcu-11-Zn- $\alpha$** .



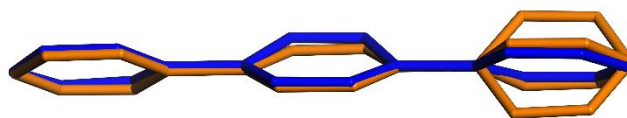
**Fig. S3** Illustrations of the position of pore diameters (approximately  $4.5 \times 6.8 \text{ \AA}^2$ , the direction is indicated by the arrows) viewed along the *c*-axis for **X-pcu-11-Zn- $\alpha$** .



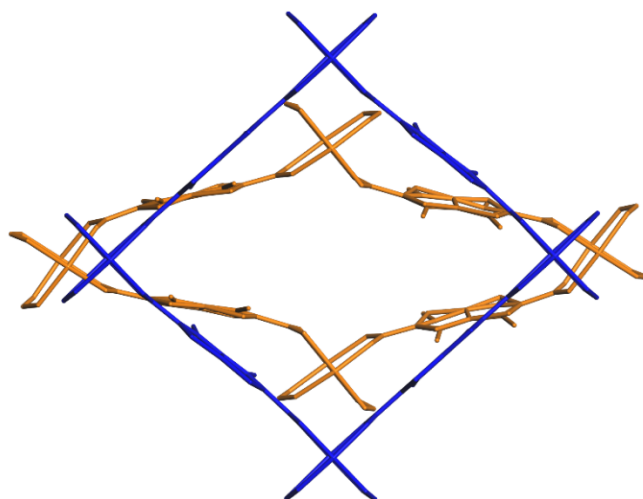
**Fig. S4** Illustrations of the position of pore diameters (approximately  $2.1 \times 2.6 \text{ \AA}^2$ , the direction is indicated by the arrows) viewed along the  $a$ -axis for **X-pcu-11-Zn- $\beta$** .



**Fig. S5** Overlay diagrams of conformations of DMTDC ligands (thieno[2,3- $b$ ]thiophene ring overlay) in **X-pcu-11-Zn- $\alpha$**  (blue) and **X-pcu-11-Zn- $\beta$**  (orange).



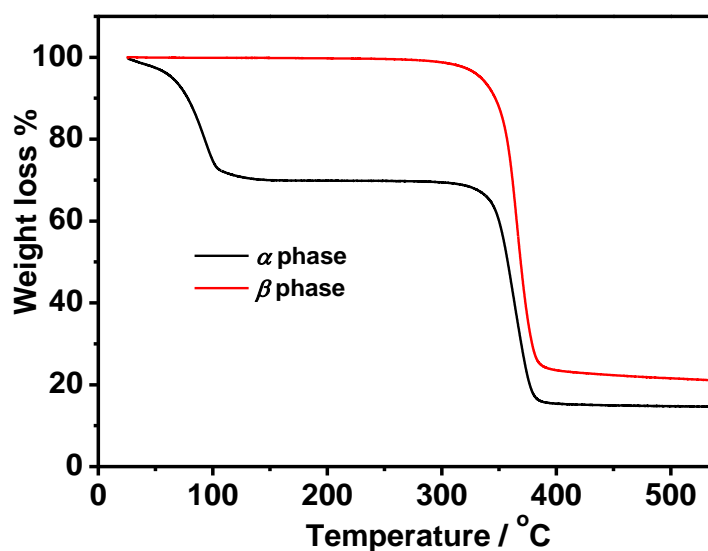
**Fig. S6** Overlay diagrams of conformations of dpb ligands (pyridyl ring overlay) in **X-pcu-11-Zn- $\alpha$**  (blue) and **X-pcu-11-Zn- $\beta$**  (orange).



**Fig. S7** Overlay diagrams of conformations of sql nets in **X-pcu-11-Zn- $\alpha$**  (blue) and **X-pcu-11-Zn- $\beta$**  (orange).

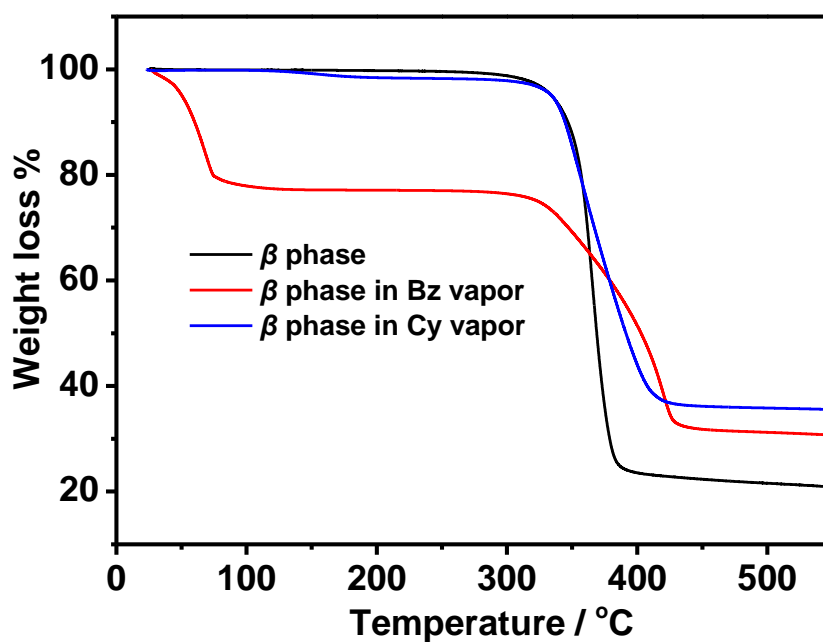
## 6. Thermogravimetric analysis (TGA).

Thermogravimetric analyses (TGA) were performed under  $N_2$  using a SDT-650 thermogravimetric analyzer system. Samples were loaded into aluminium sample pans and heated at  $10\text{ K min}^{-1}$  from room temperature to  $550^\circ\text{C}$



**Fig. S8** TG curve of **X-pcu-11-Zn- $\alpha$**  and **X-pcu-11-Zn- $\beta$**  under  $N_2$  environment The TG curve of **X-pcu-11-Zn- $\beta$**  displays a weight loss of 30.02% at  $150^\circ\text{C}$ , resulting from the release of 5

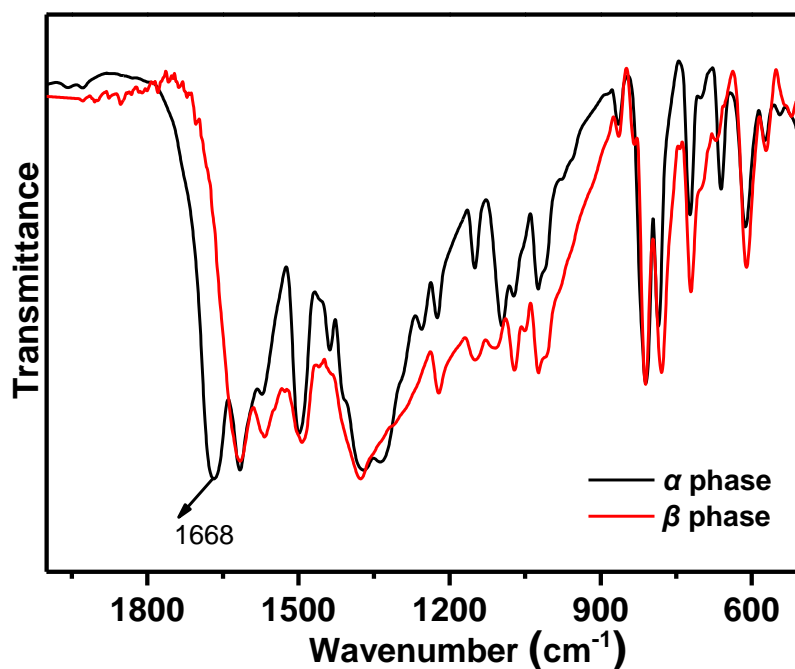
molecules of DMF and 0.5 molecules of H<sub>2</sub>O per formula unit (cal. 30.05%). The TG curve of **X-pcu-11-Zn- $\beta$**  shows no weight loss below 320 °C, indicating that there is no guest in the closed phase.



**Fig. S9** TG curve of **X-pcu-11-Zn- $\beta$**  in Bz/Cy vapor for 12 h at room temperature. The **X-pcu-9-Zn- $\beta$**  in Bz vapor weight loss (22.61%) below 115 °C can be calculated as 3.26 **Bz** molecule per molecule. TG curve of **X-pcu-11-Zn- $\beta$**  in Cy vapor displays a negligible weight loss below 300 °C (2.16%), indicating that **X-pcu-11-Zn- $\beta$**  almost cannot absorb Cy molecules.

## 7. IR spectra

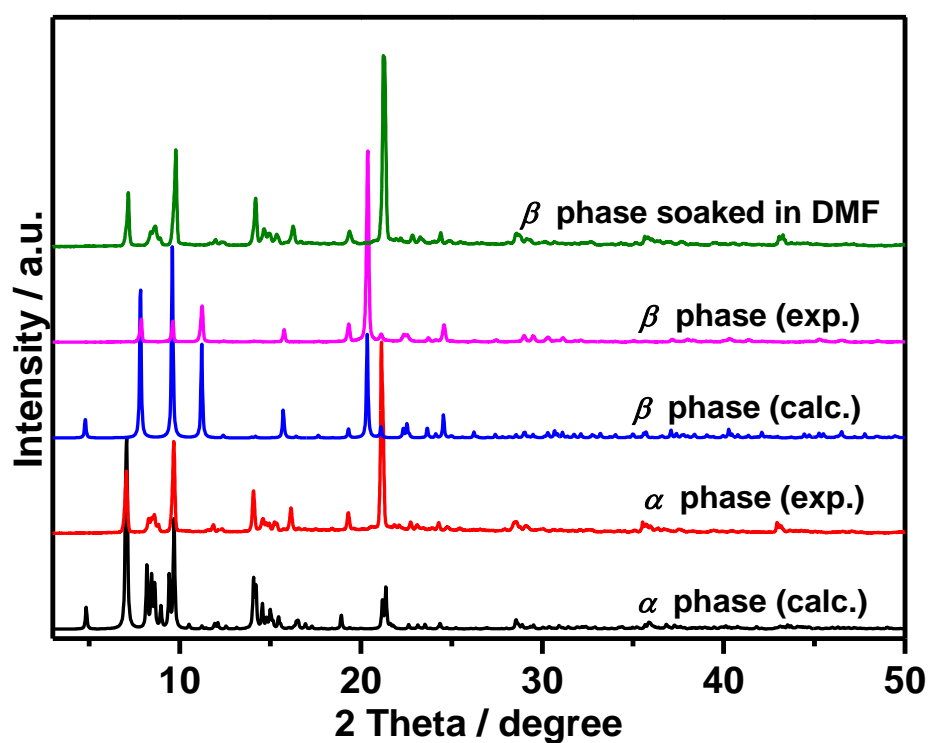
Infrared spectra were recorded from KBr pellets on a Thermo Scientific Nicolet IS 10 FTIR spectrometer in the range of 400-4000 cm<sup>-1</sup>.



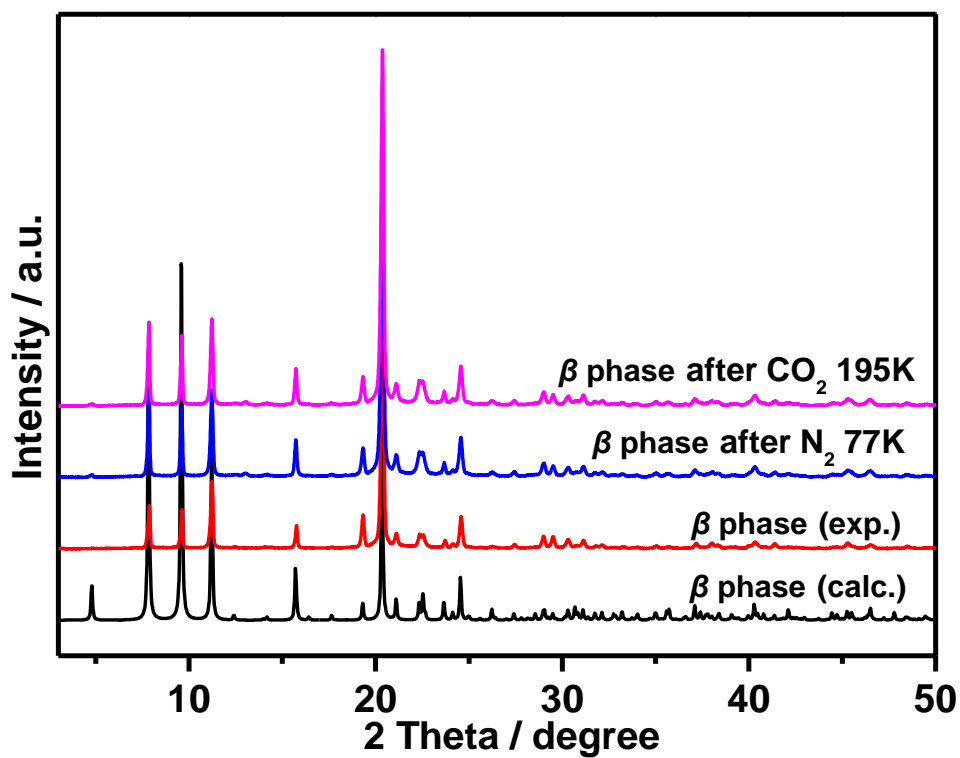
**Fig. S10** IR spectra of **X-pcu-11-Zn- $\alpha$**  and **X-pcu-11-Zn- $\beta$** . The lack of C=O stretching peak at about 1668 cm<sup>-1</sup> in the IR spectrum of **X-pcu-11-Zn- $\beta$**  also confirms the full release of DMF guests.

## 8. Powder X-ray diffraction (PXRD)

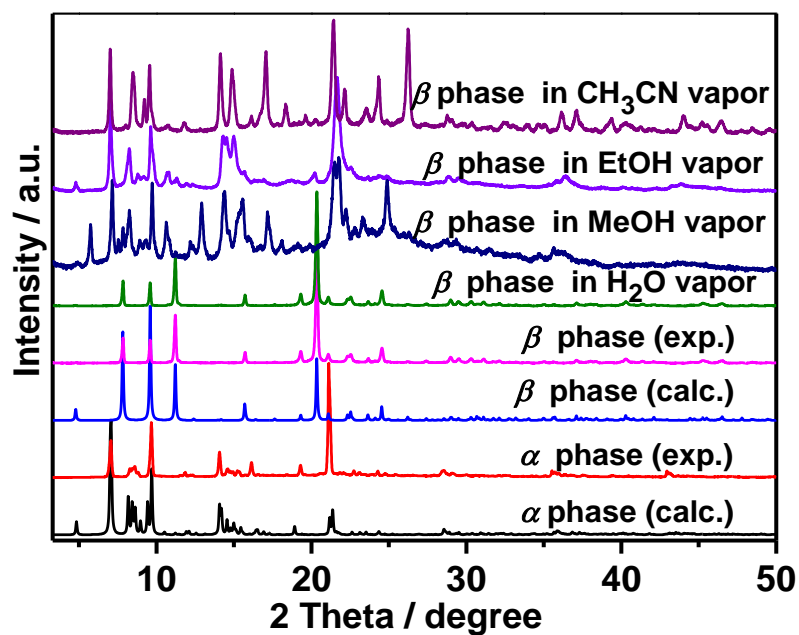
Powder X-ray diffraction (PXRD) patterns were recorded at the room temperature on a Rigaku MiniFlex600 X-ray diffractometer (40 KV, 15 mA) with Cu-K $\alpha$  ( $\lambda = 1.5405 \text{ \AA}$ ) radiation in a 2theta range from 3 to 50°. All the calculated PXRD patterns are simulated from single-crystal diffraction by using Mercury v3.8 software (Cambridge Crystallographic Data Centre, Cambridge, UK)



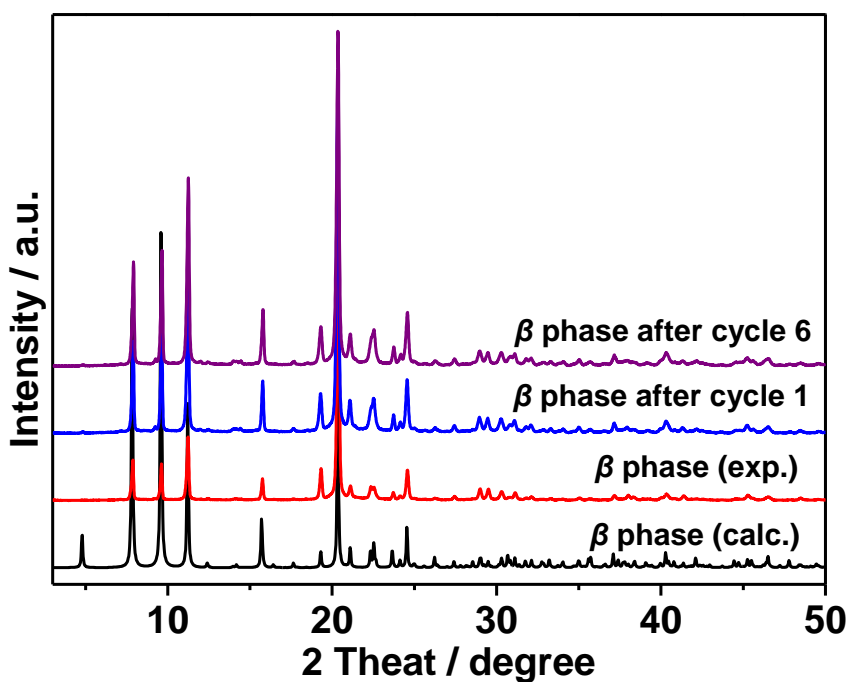
**Fig. S11** PXRD patterns of X-pcu-11-Zn- $\alpha$ , X-pcu-11-Zn- $\beta$ , and X-pcu-11-Zn- $\beta$  after soaking in DMF for one day.



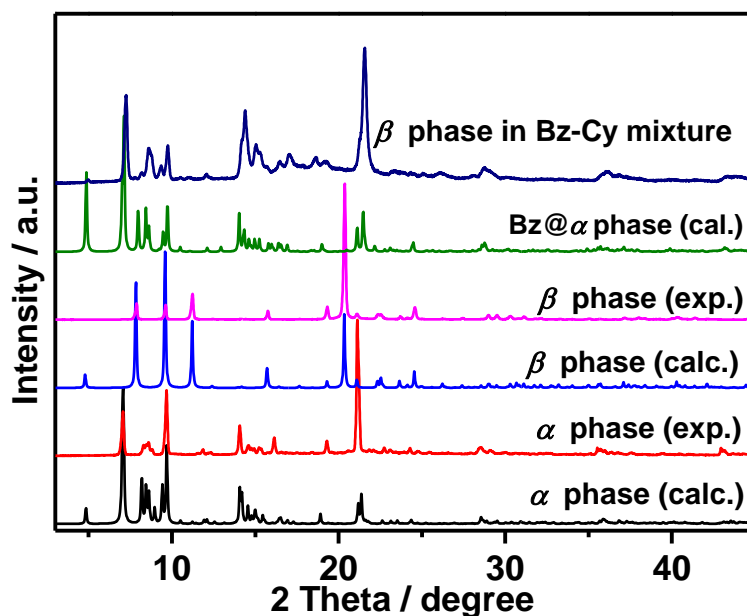
**Fig. S12** PXRD patterns of X-pcu-11-Zn- $\beta$  after gas adsorption.



**Fig. S13** PXRD patterns of **X-pcu-11-Zn- $\beta$**  in  $\text{H}_2\text{O}$ , MeOH, EtOH and  $\text{CH}_3\text{CN}$  vapour for 24 h.



**Fig. S14** PXRD patterns of **X-pcu-11-Zn- $\beta$**  after one cycle and six cycles of benzene adsorption. After each cycle of benzene sorption, the sample was heated at  $120^\circ\text{C}$  under vacuum and for the next cycle of benzene sorption.



**Fig. S15** PXRD patterns of **X-pcu-11-Zn- $\beta$**  after the exposure to an equimolar Bz/Cy mixture for 12 h.

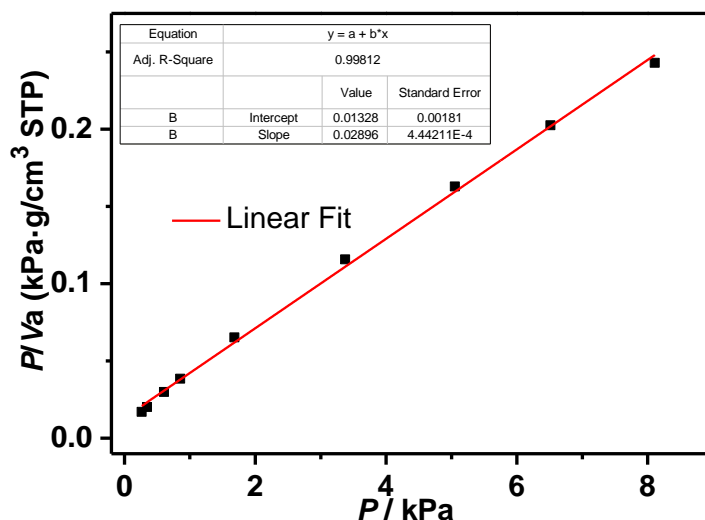
## 9. Gas and vapour adsorption measurements

All the adsorption isotherms were measured by using Belsorp-max adsorption instrument (MicrotracBEL Corp from Japan). Before sorption experiment, the samples of **X-pcu-11-Zn- $\beta$**  was placed in the quartz tube and was activated under high vacuum at 120 °C for 12 h prior to measurements. All the adsorption isotherms were tested by using relative pressure mode. The value of saturation pressure ( $P_0$ ) for gas adsorption is 80.735 kPa in Kunming (a plateau area with an altitude of about 1950 m), China. The saturated vapor pressure ( $P_0$ ) for H<sub>2</sub>O, MeOH, EtOH, MeCN, benzene, cyclohexane is 2.98, 16.24, 7.64, 11.30, 11.735 and 12.679 kPa, respectively.

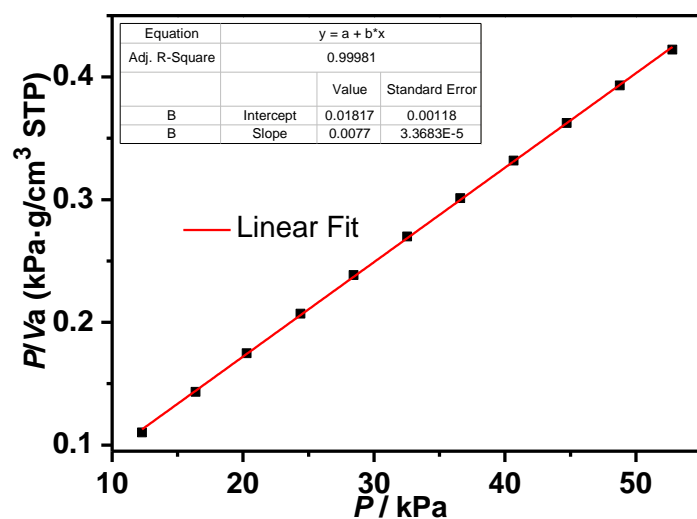
## 10. The calculation of Langmuir surface area

The surface areas of **X-pcu-11-Zn- $\beta$**  were determined from the CO<sub>2</sub> adsorption isotherm collected at 195 K by applying the Langmuir models. The surface area of the first-step CO<sub>2</sub> adsorption isotherm was determined in the range of 0.26 to 8.11 kPa (Fig. S16). The surface

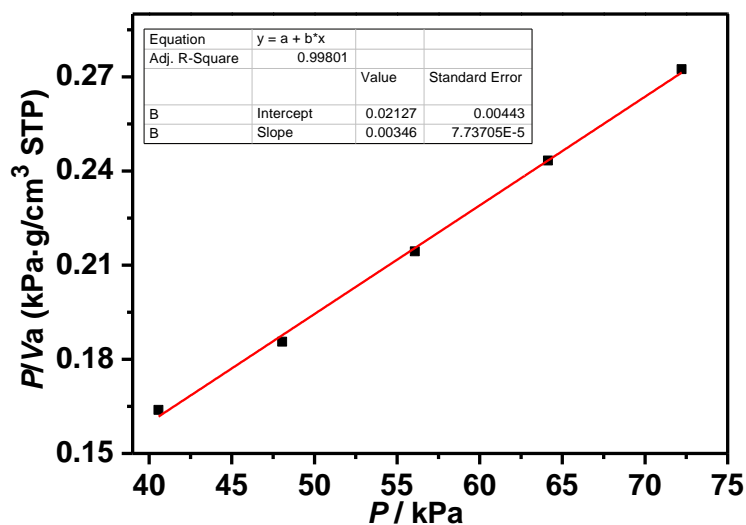
area of the second-step CO<sub>2</sub> adsorption isotherm was determined in the range of 12.28 to 52.79 kPa (Fig. S17). The surface area of the third-step CO<sub>2</sub> adsorption isotherm cannot be determined by applying the Langmuir models. Thus, we use the first-step CO<sub>2</sub> desorption isotherm in the range of 40.56 to 72.22 kPa to determine the surface area by applying the Langmuir models (Fig. S18). Note that Brunauer-Emmett-Teller (BET) surface areas cannot be accurately determined for either framework because of the switching or breathing CO<sub>2</sub> adsorption isotherms at 195 K.



**Fig. S16** Langmuir plot for the CO<sub>2</sub> adsorption isotherm of **X-pcu-11-Zn- $\beta$**  at 195 K, and the range  $P$  from 0.26 to 8.11 kPa satisfies for applying the Langmuir theory.



**Fig. S17** Langmuir plot for the CO<sub>2</sub> adsorption isotherm of **X-pcu-11-Zn- $\beta$**  at 195 K, and the range  $P$  from 12.28 to 52.79 kPa satisfies for applying the Langmuir theory.



**Fig. S18** Langmuir plot for the first-step CO<sub>2</sub> desorption branch of **X-pcu-11-Zn- $\beta$**  at 195 K, and the range  $P$  from 40.56 to 72.22 kPa satisfies for applying the Langmuir theory.

The adsorption isotherms were converted into plots of  $P/V$  vs.  $P$  for determining the appropriate range. As shown in Fig. S16-Fig. S17, the range  $P$  from 0.26 to 8.11 kPa and the range  $P$  from 12.28 to 52.79 kPa in the CO<sub>2</sub> adsorption isotherm satisfy for applying the

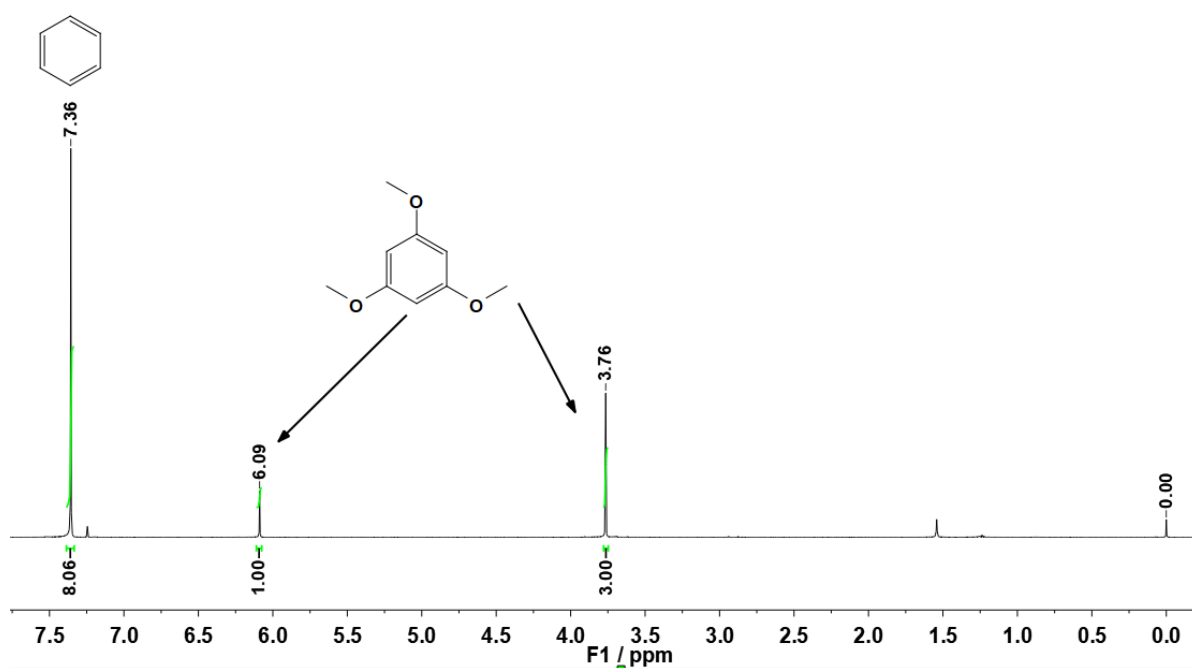
Langmuir theory. As shown in Fig. S18, the range  $P$  from 40.56 to 72.22 kPa in the CO<sub>2</sub> desorption isotherm satisfy for applying the Langmuir theory. After having identified the appropriate low pressure Langmuir  $P$  range, the analysis proceeds according to the standard method via the linearized Langmuir equation (1).

$$P/V = P/V_m + 1/BV_m \quad (1)$$

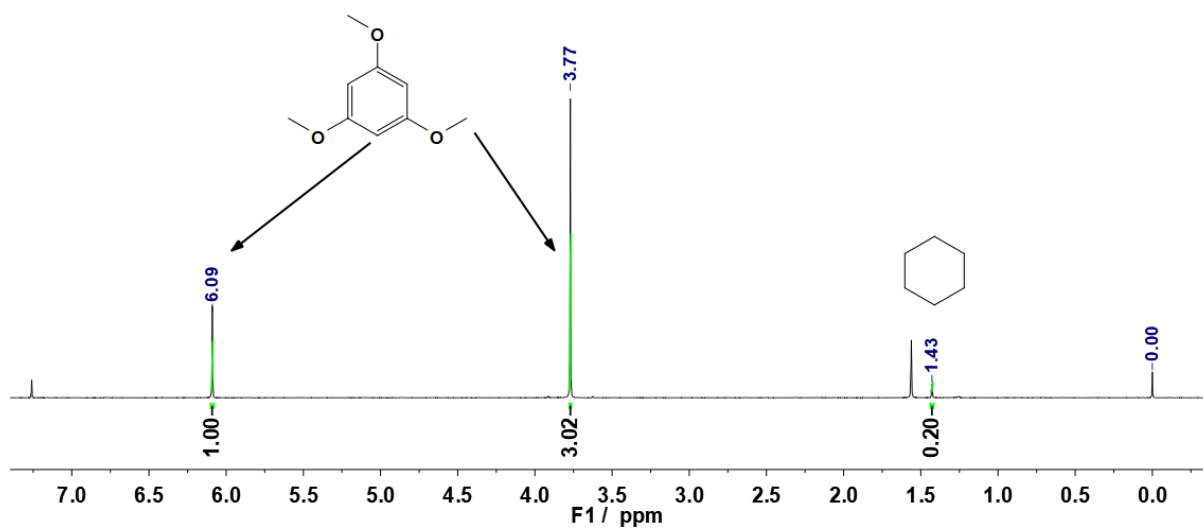
from which the parameters  $V_m$  is obtained from the relation  $V_m = 1/s$ ,  $s$  being the slope with the ordinate of the plot  $P/V$  vs.  $P$ . The surface area is then obtained from  $A_{\text{Langmuir}} = V_m \sigma_m N_A$  with  $\sigma_m$  being the cross-sectional area of CO<sub>2</sub> at liquid density ( $1.037 \times 10^{-26}$  m<sup>2</sup>), and  $N_A$  is the Avogadro's number.

## 11. Time-dependent, single-component Bz/Cy adsorption experiments

An open 5 mL vial containing 30 mg of guest-free **X-pcu-11-Zn-β** adsorbent was placed in sealed 30 mL vial respectively containing of Bz or Cy (3 mL) solvent. The diffusion in vapor keep away from light for 10, 20, 40, 60, 120, 240, 360, 480 and 720 min at room temperature. After reaching the diffusion time, the uptakes of Bz or Cy by **X-pcu-11-Zn-β** was measured at each time interval by completely soaking the samples in CDCl<sub>3</sub> (1 mL) for 48 h. The supernatant was taken for <sup>1</sup>H NMR test. <sup>1</sup>H NMR experiments were performed by using the internal standard 1,3,5-trimethoxybenzene (TMB, 5 mg) to determine the amount of absorbed Bz or Cy. <sup>1</sup>H NMR spectra were recorded at 500 MHz using a Bruker DRX 500 NMR spectrometer.



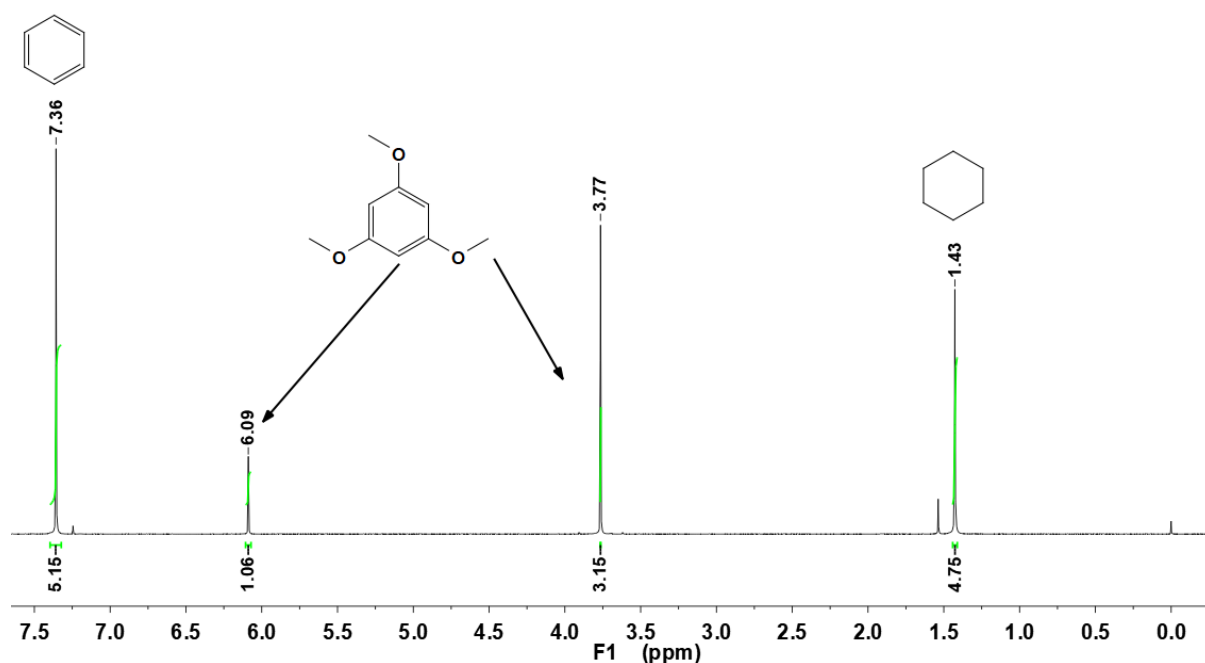
**Fig. S19**  $^1\text{H}$  NMR spectrum (500 MHz,  $\text{CDCl}_3$ , 298 K) of the absorbed benzene from **X-pcu-11-Zn- $\beta$**  under the exposure of Bz vapor for 12 h.



**Fig. S20**  $^1\text{H}$  NMR spectrum (500 MHz,  $\text{CDCl}_3$ , 298 K) of the absorbed cyclohexane from **X-pcu-11-Zn- $\beta$**  under the exposure of Cy vapor for 12 h.

## 12. Time-dependent, binary-component Bz/Cy adsorption experiments

An open 5 mL vial containing 30 mg of guest-free **X-pcu-11-Zn- $\beta$**  adsorbent was placed in sealed 30 mL vial respectively containing of an equimolar Bz/Cy mixture (3.25 mL) solvent. Then diffusion for 10, 20, 40, 60, 120, 240, 360, 480 and 720 min at room temperature and away from light. After reaching the diffusion time, the uptakes of the ratio of Bz and Cy by **X-pcu-11-Zn- $\beta$**  was measured at each time interval by completely soaking the samples in  $\text{CDCl}_3$  (1 mL) for 48 h.  $^1\text{H}$  NMR experiments were performed by using the standard 1,3,5-trimethoxybenzene(TMB) to determine the ration of absorbed Bz and Cy.



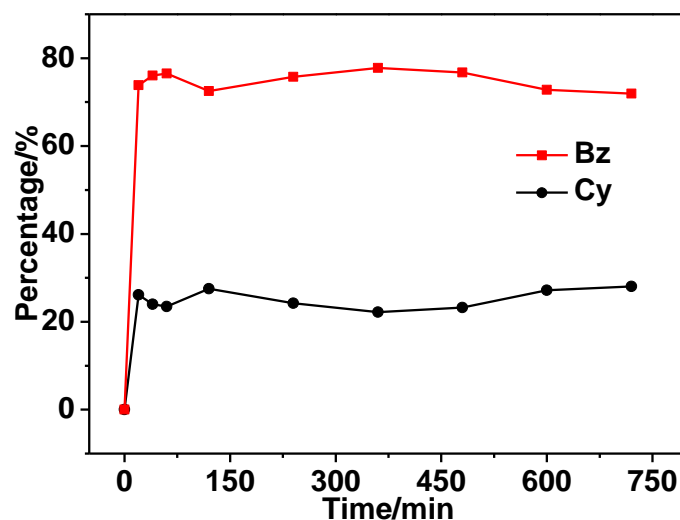
**Fig. S21**  $^1\text{H}$  NMR spectrum (500 MHz,  $\text{CDCl}_3$ , 298 K) of the absorbed benzene and cyclohexane from **X-pcu-11-Zn- $\beta$**  under the exposure of an equimolar Bz/Cy vapour (1:1) for 12 h.

### 13. Cycling tests of Bz adsorption.

An open 35 mL vial containing 300 mg and an open 5 mL vial containing 30 mg of guest-free **X-pcu-11-Zn- $\beta$**  adsorbent was placed in sealed 100 mL vial containing Bz (35 mL) solvent. After 12 h, the 5 mL vial containing 30 mg was taken out and the uptakes of Bz by **X-pcu-11-Zn- $\beta$**  was measured by completely soaking the samples in  $\text{CDCl}_3$  (1 mL) for 48 h.  $^1\text{H}$  NMR experiments were performed by using the standard 1,3,5-trimethoxybenzene(TMB) to determine the amount of absorbed Bz. After each cycle of Bz adsorption, the sample was activated at 120°C for 12 h under vacuum. The above operation was repeated for six cycles.

### 14. Binary-component Bz/Cy adsorption experiments by Gas Chromatography

An open 5 mL vial containing 30 mg of guest-free **X-pcu-11-Zn- $\beta$**  adsorbent was placed in sealed 25 mL vial respectively containing of equimolar Bz/Cy (5 mL) mixture. Then diffusion for 10, 20, 40, 60, 120, 240, 360, 480 and 720 min, at room temperature and away from light. After reaching the diffusion time, transfer the sample in the vial to the glass vial. Plug the mouth of the vial with rubber plug, and seal it with sealing glue. Then gas chromatography was used to test the adsorption content of **X-pcu-11-Zn- $\beta$**  samples at different times of solid-vapor diffusion. The procedure is as follows: place sealed vials in a constant temperature heater at 130 °C for 20 min, then extract 300  $\mu\text{L}$  with an airtight needle for content analysis. Experiments were performed on an Agilent 7820. Nitrogen (99.999%) was used as the carrier gas. Instrument parameter setting: Injector temperature 250 °C, column temperature 65 °C, detector temperature 250 °C, column temperature 170 °C, commercial column: DP-17 (0.53 mm $\times$ 25 m).



**Fig. S22** Time-dependent solid-vapor sorption plot of **X-pcu-11-Zn-β** for Bz/Cy equimolar mixture vapour according to gas chromatography.

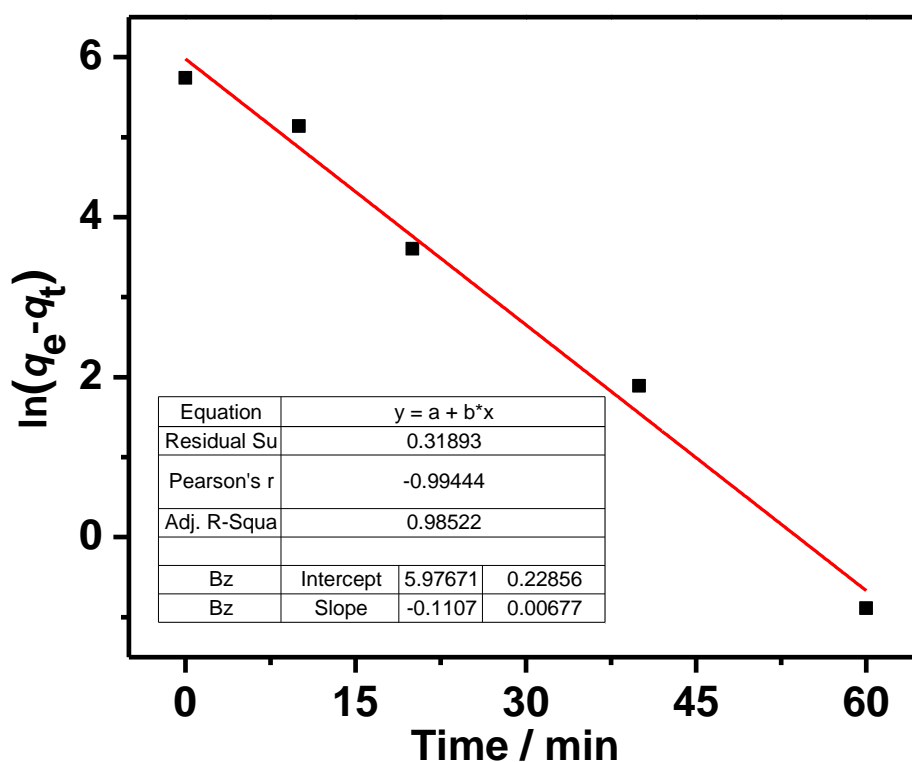
### 15. Kinetic analysis for Bz adsorption

The kinetics of **X-pcu-11-Zn-β** for the adsorption of Bz was determined by calculating the uptakes of Bz at different time intervals. The adsorbed performances ( $q_t$ ) of Bz as a function of time ( $t$ ) are shown in Fig. 7a. The uptakes for Bz increased gradually and approached equilibrium at the contact time of about 60 min (Fig. 7a). The experimental value of the saturated adsorption capacity ( $q_e$ ) for Bz is 311.58 mg g<sup>-1</sup>. Pseudo-first-order and pseudo-second-order kinetic models were used to fit the experimental data as represented by equations (2) and (3), respectively.<sup>8</sup>

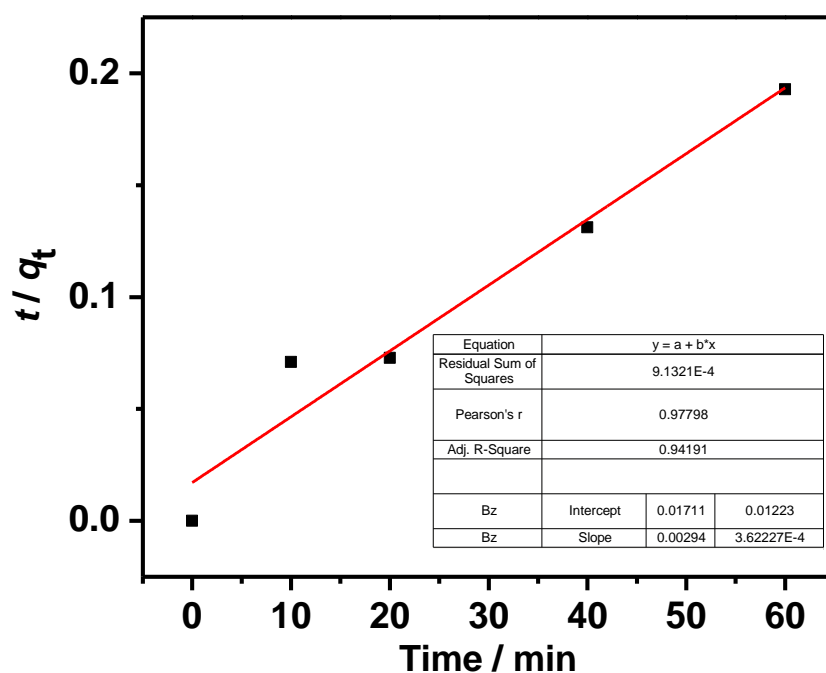
$$\ln(q_e - q_t) = \ln q_e - k_1 t \quad (2)$$

$$\frac{t}{q_t} = \frac{1}{k_2 q_e^2} + \frac{t}{q_e} \quad (3)$$

where  $k_1$  ( $\text{h}^{-1}$ ) and  $k_2$  ( $\text{g mg}^{-1} \text{h}^{-1}$ ) denote the rate constants of the pseudo-first-order and pseudo-second-order, respectively. The fitting results and correlation coefficient  $R^2$  of the models were shown in Fig. S23-S24 and Table S6, respectively. It is apparent from the values of correlation coefficients that the fitness of the pseudo-first-order model ( $R^2 = 0.9852$ ) is better as compared to pseudo-second-order model ( $R^2 = 0.9419$ ) for Bz, implying that the adsorption kinetics can be best described by the pseudo-first-order model for **X-pcu-11-Zn- $\beta$** . This suggests that the adsorption process may be governed by physisorption rather than chemisorption.



**Fig. S23** Kinetic plot of adsorption of Bz by **X-pcu-11-Zn- $\beta$**  defining pseudo-first order kinetics.



**Fig. S24** Kinetic plot of adsorption of Bz by **X-pcu-11-Zn- $\beta$**  defining pseudo-second order kinetics.

**Table S6.** Kinetics constants and correlation coefficients.

Model	Parameter	Bz
pseudo-first-order	$K_1$ ( $\text{min}^{-1}$ )	0.1107
	$q_{e,\text{exp.}}$ ( $\text{mg g}^{-1}$ )	311.58
	$q_{e,\text{cal.}}$ ( $\text{mg g}^{-1}$ )	394.14
	$R^2$	0.9852
pseudo-second-order	$K_2$ ( $\text{g mg}^{-1} \text{min}^{-1}$ )	5.052E-4
	$q_{e,\text{exp.}}$ ( $\text{mg g}^{-1}$ )	311.58
	$q_{e,\text{cal.}}$ ( $\text{mg g}^{-1}$ )	340.14
	$R^2$	0.9419

## 16. Summary of switching and breathing metal-organic materials

**Table S7.** Summary of switching adsorbent materials from closed to two open phases showing two-step adsorption.

Materials	Triggered gas	Saturated Uptake (cm <sup>3</sup> /g)	Pressure of gate opening for 1 <sup>st</sup> step	Pressure of gate opening for 2 <sup>nd</sup> step	Ref.
<b>X-pcu-11-Zn-<math>\beta</math></b>	N <sub>2</sub>	337 (77 K) <sup>a</sup>	$P/P_0 = 0.10$	$P/P_0 = 0.46$	This work
<b>MIL-53(Sc)</b>	CO <sub>2</sub>	~291 (196 K) <sup>a</sup>	$P = 0.05$ bar	$P = 0.75$ bar	9
<b>MIL-53(Fe)</b>	C <sub>2</sub> H <sub>6</sub>	~148 (303 K) <sup>b</sup>	$P \approx 0.9$ bar	$P \approx 9$ bar	10
	C <sub>3</sub> H <sub>8</sub>	~90 (303 K) <sup>b</sup>	$P \approx 0.5$ bar	$P \approx 8$ bar	
<b>[Zn(pydc)(dma)]</b>	Ar	245 (87 K) <sup>a</sup>	$P = 17$ KPa	$P = 41$ KPa	11
<b>RPM3-Zn</b>	CO <sub>2</sub>	~58 (195 K) <sup>a</sup>	$P \approx 0.0008$ bar	$P \approx 0.005$ bar	12
	CO <sub>2</sub>	~58 (185 K) <sup>a</sup>	$P \approx 0.0003$ bar	$P \approx 0.002$ bar	
	CO <sub>2</sub>	~58 (234 K) <sup>a</sup>	$P \approx 0.0025$ bar	$P \approx 0.1$ bar	
	CO <sub>2</sub>	~58 (273 K) <sup>a</sup>	$P \approx 0.03$ bar	$P \approx 1$ bar	
	C <sub>3</sub> H <sub>8</sub>	~50 (298 K) <sup>a</sup>	$P \approx 0.005$ atm	$P \approx 0.18$ atm	13
	C <sub>4</sub> H <sub>10</sub>	~53 (298 K) <sup>a</sup>	$P \approx 0.06$ atm	$P \approx 0.15$ atm	
<b>[Zn(Hmpba)<sub>2</sub>]-1</b>	CO <sub>2</sub>	84 (77 K) <sup>a</sup>	$P/P_0 \approx 0.08$	$P/P_0 \approx 0.9$	14
<b>JLU-Liu33L</b>	N <sub>2</sub>	290 (77 K) <sup>a</sup>	$P/P_0 = 0.12$	$P/P_0 = 0.89$	15
<b>ELM-13</b>	C <sub>2</sub> H <sub>2</sub>	71.8 (273 K) <sup>a</sup>	$P = 0.03$ bar	$P = 0.25$ bar	16
	C <sub>2</sub> H <sub>2</sub>	~60 (298 K) <sup>a</sup>	$P = 0.07$ bar	$P = 0.55$ bar	
<b>ELM-11</b>	C <sub>2</sub> H <sub>2</sub>	82.2 (273 K) <sup>a</sup>	$P = 0.04$ bar	$P = 0.25$ bar	
	C <sub>2</sub> H <sub>2</sub>	~80 (298 K) <sup>a</sup>	$P = 0.1$ bar	$P = 0.55$ bar	
	CO <sub>2</sub>	~420 (195 K) <sup>a</sup>	$P \approx 0.25$ KPa	$P \approx 25$ KPa	17
<b>sql-1-Cu-BF<sub>4</sub></b>	C <sub>2</sub> H <sub>2</sub>	~82 (283 K) <sup>a</sup>	$P = 3.8$ KPa	$P = 32.0$ KPa	18
	C <sub>2</sub> H <sub>2</sub>	~82 (288 K) <sup>a</sup>	$P = 4.8$ KPa	$P = 40.5$ KPa	
<b>SIFSIX-23-Cu-<math>\beta</math>1</b>	CO <sub>2</sub>	216 (195 K) <sup>a</sup>	$P = 2.4$ mmHg	$P \approx 28$ mmHg	19

<sup>a</sup> low pressure; <sup>b</sup> high pressure

**Table S8.** Summary of breathing adsorbent materials from open to two more open phases showing three-step adsorption.

Materials	Triggered gas	Saturated Uptake (cm <sup>3</sup> /g)	Pressure of 1 <sup>st</sup> gate opening	Pressure of 2 <sup>nd</sup> gate opening	Ref.
X-pcu-11-Zn- $\beta$	CO <sub>2</sub>	267 (195 K) <sup>a</sup>	$P/P_0 = 0.10$	$P/P_0 = 0.70$	This work
SNU-9	N <sub>2</sub>	262 (77 K) <sup>a</sup>	$P = 0.001$ atm	$P = 0.019$ atm	20
	N <sub>2</sub>	~240 (87 K) <sup>a</sup>	$P \approx 0.003$ atm	$P \approx 0.01$ atm	
	O <sub>2</sub>	360 (77 K) <sup>a</sup>	$P = 0.00045$ atm	$P = 0.014$ atm	
	O <sub>2</sub>	275 (87 K) <sup>a</sup>	$P = 0.0016$ atm	$P = 0.003$ atm	
	CO <sub>2</sub>	219 (195 K) <sup>a</sup>	$P = 0.026$ atm	$P = 0.16$ atm	
[Cu(bpy) <sub>2</sub> (OTf) <sub>2</sub> ] <sub>n</sub>	N <sub>2</sub>	~179 (77 K) <sup>a</sup>	$P/P_0 \approx 0.002$	$P/P_0 \approx 0.16$	21
	CO <sub>2</sub>	~184 (196 K) <sup>a</sup>	$P/P_0 \approx 0.06$	$P/P_0 \approx 0.26$	
	Ar	~269 (87 K) <sup>a</sup>	$P/P_0 = 0.15$	$P/P_0 \approx 0.30$	
[Zn <sub>2</sub> (tp) <sub>2</sub> (L <sup>2</sup> ) <sub>n</sub> ]	CO <sub>2</sub>	~245 (195 K) <sup>a</sup>	$P = 5$ KPa	$P = 40$ KPa	22
[Cu <sub>4</sub> ( $\mu_4$ -O)( $\mu_2$ -OH) <sub>2</sub> (Me <sub>2</sub> trzpbpa) <sub>4</sub> ]-1a	N <sub>2</sub>	~350 (77 K) <sup>a</sup>	$P/P_0 \approx 0.5$	$P/P_0 \approx 0.72$	23
[Cu <sub>4</sub> ( $\mu_4$ -O)( $\mu_2$ -OH) <sub>2</sub> (Me <sub>2</sub> trzpbpa) <sub>4</sub> ]-1,2	N <sub>2</sub>	~380 (77 K) <sup>a</sup>	$P/P_0 \approx 0.001$	$P/P_0 \approx 0.43$	
[Cu <sub>4</sub> ( $\mu_4$ -O)( $\mu_2$ -OH) <sub>2</sub> (Me <sub>2</sub> trzpbpa) <sub>4</sub> ]-1	Ar	~410 (77 K) <sup>a</sup>	$P/P_0 \approx 0.007$	$P/P_0 \approx 0.13$	
[Zn(Hmpba) <sub>2</sub> ]-2	N <sub>2</sub>	~130 (77 K) <sup>a</sup>	$P/P_0 \approx 0.00002$	$P/P_0 \approx 0.60$	14
	CO <sub>2</sub>	~100 (195 K) <sup>a</sup>	$P/P_0 \approx 0.002$	$P/P_0 \approx 0.20$	
[Cd <sub>1.5</sub> (bmip)(tpa) <sub>1.5</sub> ·(DMF) <sub>1.5</sub> ]	CO <sub>2</sub>	70.8 (195 K) <sup>a</sup>	$P/P_0 = 0.04$	$P/P_0 = 0.60$	24
JLU-Liu33L	CO <sub>2</sub>	~225 (195 K) <sup>a</sup>	$P/P_0 = 0.02$	$P/P_0 = 0.3$	15
[Cd <sub>2</sub> (NH <sub>2</sub> iso) <sub>2</sub> (tdih) <sub>2</sub> ] 4 DMF H <sub>2</sub> O	CO <sub>2</sub>	216 (195 K) <sup>a</sup>	$P/P_0 = 0.43$	$P/P_0 = 0.59$	25
[Zn <sub>2</sub> (NH <sub>2</sub> iso) <sub>2</sub> (tdih) <sub>2</sub> ] 2D MF 3H <sub>2</sub> O	CO <sub>2</sub>	130 (195 K) <sup>a</sup>	$P/P_0 = 0.09$	$P/P_0 = 0.43$	
MIL-101	N <sub>2</sub>	~1080 (77 K) <sup>a</sup>	$P/P_0 \approx 0.10$	$P/P_0 \approx 0.20$	26
MIL-53(Al)	CH <sub>4</sub>	~79 (213 K) <sup>b</sup>	$P \approx 0.25$ bar	$P \approx 1.5$ bar	27
MHP-P5Q	N <sub>2</sub>	~85 (77 K) <sup>a</sup>	$P/P_0 \approx 0.08$	$P/P_0 \approx 0.18$	28
NOTT-202a	CO <sub>2</sub>	448 (195 K) <sup>a</sup>	$P/P_0 \approx 0.42$	$P/P_0 \approx 0.82$	29
[Zn(Gly-Ala) <sub>2</sub> ]	CO <sub>2</sub>	~97 (273 K) <sup>b</sup>	$P = 2$ bar	$P \approx 10$ bar	30
RPM4-Zn	CO <sub>2</sub>	27.7 (298 K) <sup>a</sup>	$P = 0.08$ bar	$P = 0.6$ bar	31
	CO <sub>2</sub>	~40 (273 K) <sup>a</sup>	$P = 0.05$ bar	$P = 0.25$ bar	
[Zn( <sup>HBC</sup> L)(DEF)] <sub>n</sub>	C <sub>2</sub> H <sub>2</sub>	~358 (189 K) <sup>a</sup>	$P/P_0 = 0.11$	$P/P_0 = 0.58$	32
sql-1-Cu-BF <sub>4</sub>	C <sub>2</sub> H <sub>2</sub>	325 (195 K) <sup>a</sup>	$P \approx 3$ KPa	$P \approx 45$ KPa	18

<sup>a</sup> low pressure; <sup>b</sup> high pressure

**Table S9.** Comparison on Bz/Cy separation performances for selected flexible MOFs.

FMOFs	Benzene Saturate Uptake (cm <sup>3</sup> /g)	Cyclohexane Saturate Uptake (cm <sup>3</sup> /g)	Benzene/cyclohexane selectivity	Reusability	Host-guest interactions	Ref
X-pcu-11-Zn- $\beta$	92	5	18.4 (isotherms); 2.16:1 (1:1 vapor mixture)	yes	$\pi\cdots\pi$ and C-H $\cdots\pi$ interactions with Bz	This work
[Zn( $\mu_4$ -TCNQ-TCNQ)bpy]	~80	~20	~4:1 (isotherms); 24:1 (1:1 vapor mixture)	yes	C-H $\cdots\pi$ interactions with Bz	33
MAF-2	59.1	2.4	24.6:1 (isotherms)	no	C-H $\cdots\pi$ interactions with Bz	34
[ZnL]	33.8	5.9	~5.7:1 (isotherms); ~32.3:1 (1:1 liquid mixture)	yes	C-H $\cdots\pi$ interactions with Bz	35
MAF-24 $\beta$	57.6	4.4	~13:1 (isotherms)	no	C-H $\cdots\pi$ and $\pi\cdots\pi$ interactions with Bz	36
[Mn(TCNQ-TCNQ)bpy] <sub>n</sub>	~80	~40	~2:1 (isotherms); 19:1 (1:1 vapor mixture)	yes	C-H $\cdots\pi$ interactions with Bz	37
Ni <sub>3</sub> (OH)(Ina) <sub>3</sub> (BDC) <sub>1.5</sub>	~65	~3.7	~17.5:1 (isotherms)	no	$\pi\cdots\pi$ interactions with Bz	38
CID-23	27	2	13.5:1 (isotherms); 25:1 (1:1 vapor mixture)	no	C-H $\cdots\pi$ interactions with Bz	39
[Co(pybz) <sub>2</sub> ]	~51	~23	2:1 (isotherms)	no	/	40
[Zn <sub>2</sub> L <sub>2</sub> (DMF) <sub>2</sub> ]	29.1	9.7	~3:1 (isotherms)	no	$\pi\cdots\pi$ interactions with Bz facilitated by $\pi$ -electron deficient linker	41
CuL <sub>2</sub> (NO <sub>3</sub> ) <sub>2</sub>	45.9	6.3	~7.3:1 (isotherms); Benzene>>cyclohexane (1:1 vapor mixture)	no	$\pi\cdots\pi$ and C-H $\cdots\pi$ interactions promoted by conjugated aromatic ligands and basic amide group	42
DAT-MOF-1	~38.1	~4.7	~8:1 (isotherms); >200 (IAST, 1:1 vapor mixture)	no	$\pi$ -electron deficient diamino-triazine linker driven Bz selective interactions	43
[Cu(bpp) <sub>2</sub> (BF <sub>4</sub> ) <sub>2</sub> ]	71.1	1.6	~44.4:1 (isotherms); 1:1 (1:1 liquid mixture)	no	bpp linker movement based flexible MOF, influenced by C-H $\cdots\pi$ interactions.	44
{[Cd(ATAIA)] 4H <sub>2</sub> O} <sub>n</sub>	52	8	~6.5:1 (isotherms)	no	interactions between $\pi$ -electron deficient triazine ligand and Bz	45

## References

1. B. A. Coombs, S. R. Rutter, A. E. Goeta, H. A. Sparkes, A. S. Batsanov, A. Beeby, *RSC Adv.* 2012, **2**, 1870-1876.
2. APEX3. Ver. 2017.3-0. Bruker AXS Inc., Madison, Wisconsin, USA, 2017.
3. G. M. Sheldrick, SADABS, A program for area detector absorption corrections, University of Göttingen, Germany, 1994.
4. T. Higashi, ABSCOR, Program for Bruker area detector absorption correction, Rigaku Corporation, Tokyo, Japan, 1995.
5. Sheldrick, G. *Acta Cryst. A* **2015**, *71*, 3-8.
6. Sheldrick, G. *Acta Cryst. C* **2015**, *71*, 3-8.
7. (a) Spek, A. L. *J. Appl. Crystallogr.* 2003, *36*, 7-13; (b) Spek, A. L. *PLATON, Molecular Geometry Program*, University of Utrecht, The Netherlands, 1999.
8. L. Ullah, G. Zhao, N. Hedin, X. Ding, S. Zhang, X. Yao, Y. Nie and Y. Zhang, *Chem. Eng. J.*, 2019, **362**, 30-40.
9. L. Chen, J. P. S. Mowat, D. Fairen-Jimenez, C. A. Morrison, S. P. Thompson, P. A. Wright and Tina Düren, *J. Am. Chem. Soc.*, 2013, **135**, 15763-15773.
10. P. L. Llewellyn, P. Horcajada, G. Maurin, T. Devic, N. Rosenbach, S. Bourrelly, C. Serre, D. Vincent, S. Loera-Serna, Y. Filinchuk and G. Férey, *J. Am. Chem. Soc.*, 2009, **131**, 13002-13008.
11. H. Chun and J. Seo, *Inorg. Chem.*, 2009, **48**, 9980-9982.
12. H. Wu, C. G. Thibault, H. Wang, K. A. Cychosz, M. Thommes and J. Li, *Microporous Mesoporous Mater.*, 2016, **219**, 186-189.
13. N. Nijem, H. Wu, P. Canepa, A. Marti, K. J. Balkus, Jr., T. Thonhauser, J. Li and Y. J. Chabal, *J. Am. Chem. Soc.*, 2012, **134**, 15201-15204.
14. C.-T. He, P.-Q. Liao, D.-D. Zhou, B.-Y. Wang, W.-X. Zhang, J.-P. Zhang and X.-M. Chen, *Chem. Sci.*, 2014, **5**, 4755-4762.
15. X. Sun, S. Yao, G. Li, L. Zhang, Q. Huo, and Y. Liu, *Inorg. Chem.*, 2017, **56**, 6645-6651.
16. L. Li, R. Krishna, Y. Wang, X. Wang, J. Yang and J. Li, *Eur. J. Inorg. Chem.*, 2016, **2016**, 4457-4462.

17. S. Hiraide, H. Tanaka, N. Ishikawa and M. T. Miyahara, *ACS Appl. Mater. Interfaces*, 2017, **9**, 41066-41077.
18. S.-Q. Wang, X.-Q. Meng, M. Vandichel, S. Darwish, Z. Chang, X.-H. Bu and M. J. Zaworotko, *ACS Appl. Mater. Interfaces*, 2021, **13**, 23877-23883.
19. B.-Q. Song, Q.-Y. Yang, S.-Q. Wang, M. Vandichel, A. Kumar, C. M. Crowley, N. Kumar, C.-H. Deng, V. G. Perez, M. Lusi, H. Wu, W. Zhou and M. J. Zaworotko, *J. Am. Chem. Soc.*, 2020, **142**, 6896-6901.
20. H. J. Park and M. P. Suh, *Chem. Commun.*, 2010, **46**, 610-612.
21. A. Kondo, H. Kajiro, H. Noguchi, L. Carlucci, D. M. Proserpio, G. Ciani, K. Kato, M. Takata, H. Seki, M. Sakamoto, Y. Hattori, F. Okino, K. Maeda, T. Ohba, K. Kaneko and H. Kanoh, *J. Am. Chem. Soc.*, 2011, **133**, 10512-10522.
22. J. Seo, C. Bonneau, R. Matsuda, M. Takata and S. Kitagawa, *J. Am. Chem. Soc.*, 2011, **133**, 9005-9013.
23. C. Reichenbach, G. Kalies, J. Lincke, D. Lässig, H. Krautscheid, J. Moellmer and M. Thommes, *Micropor. Mesopor. Mater.*, 2011, **142**, 592-600.
24. J.-T. Shi, K.-F. Yue, B. Liu, C.-S. Zhou, Y.-L. Liu, Z.-G. Fang and Y.-Y. Wang, *CrystEngComm*, 2014, **16**, 3097-3102.
25. K. Roztocki, M. Szufla, V. Bon, I. Senkovska, S. Kaskel and D. Matoga, *Inorg. Chem.*, 2020, **59**, 10717-10726.
26. K. Yanagita, J. Hwang, J. A. Shamim, W.-L. Hsu, R. Matsuda, A. Endo, J.-J. Delaunay and H. Daiguji, *J. Phys. Chem. C*, 2019, **123**, 387-398.
27. A. Boutin, F.-X. Coudert, M.-A. Springuel-Huet, A. V. Neimark, G. Férey and A. H. Fuchs, *J. Phys. Chem. C*, 2010, **114**, 22237-22244.
28. K. Jie, Y. Zhou, Q. Sun, B. Li, R. Zhao, D. Jiang, Wei Guo, H. Chen, Z. Yang, F. Huang and S. Dai, *Nat. Commun.*, 2020, **11**, 1086.
29. S. Yang, X. Lin, W. Lewis, M. Suyetin, E. Bichoutskaia<sup>1</sup>, J. E. Parker, C. C. Tang, D. R. Allan, P. J. Rizkallah, P. Hubberstey, N. R. Champness, K. M. Thomas, A. J. Blake and M. Schröder, *Nat. Mater.*, 2012, **11**, 710-716.

30. J. Rabone, Y. F. Yue, S. Y. Chong, K. C. Stylianou, J. Bacsá, D. Bradshaw, G. R. Darling, N. G. Berry, Y. Z. Khimyak, A. Y. Ganin, P. Wiper, J. B. Claridge and M. J. Rosseinsky, *Science*, 2010, **329**, 1053-1057.
31. H. Wang, J. Peng, and J. Li, *Chem. Rec.*, 2016, **16**, 1298-1310.
32. S. Suginome, H. Sato, A. Hori, A. Mishima, Y. Harada, S. Kusaka, R. Matsuda, J. Pirillo, Y. Hijikata and T. Aida, *J. Am. Chem. Soc.*, 2019, **141**, 15649-15655.
33. S. Shimomura, S. Horike, R. Matsuda and S. Kitagawa, *J. Am. Chem. Soc.*, 2007, **129**, 10990-10991.
34. J.-P. Zhang and X.-M. Chen, *J. Am. Chem. Soc.*, 2008, **130**, 6010-6017.
35. G. Li, C. Zhu, X. Xi and Y. Cui, *Chem. Commun.*, 2009, 2118-2120.
36. J.-B. Lin, J.-P. Zhang, W.-X. Zhang, W. Xue, D.-X. Xue and X.-M. Chen, *Inorg. Chem.*, 2009, **48**, 6652-6660.
37. S. Shimomura, R. Matsuda and S. Kitagawa, *Chem. Mater.*, 2010, **22**, 4129-4131.
38. G. Ren, S. Liu, F. Ma, F. Wei, Q. Tang, Y. Yang, D. Liang, S. Li and Y. Chen, *J. Mater. Chem.*, 2011, **21**, 15909-15913.
39. Y. Hijikata, S. Horike, M. Sugimoto, H. Sato, R. Matsuda and S. Kitagawa, *Chem. Eur. J.*, 2011, **17**, 5138-5144.
40. M.-H. Zeng, Y.-X. Tan, Y.-P. He, Z. Yin, Q. Chen and M. Kurmoo, *Inorg. Chem.*, 2013, **52**, 2353-2360.
41. B. Joarder, S. Mukherjee, A. K. Chaudhari, A. V. Desai, B. Manna and S. K. Ghosh, *Chem. Eur. J.*, 2014, **20**, 15303-15308.
42. A. Karmakar, A. V. Desai, B. Manna, B. Joarder and S. K. Ghosh, *Chem. Eur. J.*, 2015, **21**, 7071-7076.
43. B. Manna, S. Mukherjee, A. V. Desai, S. Sharma, R. Krishnab and S. K. Ghosh, *Chem. Commun.*, 2015, **51**, 15386-15389.
44. A. Kondo, T. Suzuki, R. Kotani and K. Maeda, *Dalton Trans.*, 2017, **46**, 6762-6768.
45. P. Das and S. K. Mandal, *ACS Appl. Mater. Interfaces*, 2018, **10**, 25360-25371.